states. This can be seen, for example, as a finite zero-bias conductance in tunneling spectroscopy, and may be responsible for the excess quasi-particles identified in bulk measurements.

The above data give direct evidence of a strong source of low-energy quasi-particle excitations in BSCCO even at low temperatures. The observed QPSR characteristics, including breaking of particle-hole symmetry, diameter of $2\xi_0$, and LDOS decay as $1/r^2$, are all consistent with strong quasi-particle scattering from atomic-scale scatterers in a *d*-wave (but not *s*-wave) superconductor. Finally, this experiment demonstrates the possibility of using a single atomic-scale scatterer as a probe of high-T_c superconductivity. This technique might eventually be used, with specific elemental impurities deliberately doped into different atomic planes, to help unlock the secrets of the mechanism of high-T_c superconductivity.

Note added in proof: Since the submission of this manuscript, the authors have become aware of a recent study on atomic-scale impurities (*32*).

References and Notes

1. M. A. Woolf and F. Reif, *Phys. Rev.* **137**, A557 (1965).
2. A. A. Abrikosov and L. P. Gor'kov, *Zh. Eksp. Teor. Fiz.* **39**, 1781 (1960); *Sov. Phys. JETP* **12**, 1243 (1961).
3. H. Hancotte, R. Deltour, D. N. Davydov, A. G. M. Jansen, P. Wyder, *Phys. Rev. B* **55**, R3410 (1997).
4. R. Noetzel and K. Westerholt, *ibid.* **58**, 15108 (1998).
5. P. J. White *et al.*, http://xxx.lanl.gov/abs/cond-mat/9901349
6. A. V. Balatsky and M. I. Salkola, *Phys. Rev. Lett.* **76**, 2386 (1996), and references therein.
7. J. M. Byers, M. E. Flatté, D. J. Scalapino, *ibid.* **71**, 3363 (1993).
8. M. I. Salkola, A. V. Balatsky, D. J. Scalapino, *ibid.* **77**, 1841 (1996).
9. A. P. Kampf and T. P. Devereaux, *Phys. Rev. B* **56**, 2360 (1997).
10. M. E. Flatté and J. M. Byers, *ibid.*, p. 11213.
11. ———, *Phys. Rev. Lett.* **80**, 4546 (1998).
12. M. I. Salkola and J. R. Schrieffer, *Phys. Rev. B* **58**, R5952 (1998).
13. P. A. Lee, *Phys. Rev. Lett.* **71**, 1887 (1993).
14. A. V. Balatsky, A. Rosengren, B. L. Altshuler, *ibid.* **73**, 720 (1994).
15. M. Franz, C. Kallin, A. J. Berlinsky, *Phys. Rev. B* **54**, R6897 (1996).
16. R. Joynt, *J. Low Temp. Phys.* **109**, 811 (1997).
17. K. Ziegler, M. H. Hettler, P. J. Hirschfeld, *Phys. Rev. Lett.* **77**, 3013 (1996).
18. A. Yazdani, B. A. Jones, C. P. Lutz, M. F. Crommie, D. M. Eigler, *Science* **275**, 1767 (1997).
19. H. L. Edwards, D. J. Derro, A. L. Barr, J. T. Markert, A. L. de Lozanne, *Phys. Rev. Lett.* **75**, 1387 (1995).
20. S. H. Pan, E. W. Hudson, J. C. Davis, *Rev. Sci. Instrum.* **70**, 1459 (1999).
21. For an introduction to STM, see C. J. Chen, *Introduction to Scanning Tunneling Microscopy* (Oxford Univ. Press, Oxford, 1993).
22. No difference was observed between W and PtIr tips. In both cases, the chemical identity of the last atom on the tip is unknown.
23. D. B. Mitzi, L. W. Lombardo, A. Kapitulnik, S. S. Laderman, R. D. Jacowitz, *Phys. Rev. B* **41**, 6564 (1990).
24. S. H. Pan, E. W. Hudson, J. Ma, J. C. Davis, *Appl. Phys. Lett.* **73**, 58 (1998).
25. M. D. Kirk *et al.*, *Science* **242**, 1673 (1988).
26. Y. Gao, P. Lee, P. Coppens, M. A. Subramanian, A. W. Sleight, *ibid.* **241**, 954 (1988).
27. The value Δ, defined for this purpose as half the distance between the two coherent quasi-particle peaks, varies from 25 to 45 mV over the observed surface, with a typical value of $\Delta_0 = 32$ mV.
28. A. Pomar, M. V. Ramallo, J. Mosqueira, C. Torrón, F. Vidal, *Phys. Rev B* **54**, 7470 (1996).
29. R. Movshovich *et al.*, *Phys. Rev. Lett.* **80**, 1968 (1998).
30. S. F. Lee *et al.*, *ibid.* **77**, 735 (1996).
31. R. Mallozzi, J. Corson, J. Orenstein, J. N. Eckstein, I. Bozovic, *J. Phys. Chem. Solids* **59**, 2095 (1998).
32. A. Yazdani, C. M. Howald, C. P. Lutz, A. Kapitulnik, D. M. Eigler, *Phys. Rev. Lett.*, in press; A. Yazdani *et al.*, http://xxx.lanl.gov/abs/cond-mat/9906001.

33. We acknowledge and thank A. Balatsky, M. Flatté, M. Franz, A. de Lozanne, K. Moler, J. Orenstein, R. E. Packard, and D. J. Scalapino for helpful conversations. Funded by NSF under grants DMR-9458015 and DMR-9623842, by the D. & L. Packard Foundation, and by the U.S. Department of Energy.

19 March 1999; accepted 19 May 1999

High H_2 Uptake by Alkali-Doped Carbon Nanotubes Under Ambient Pressure and Moderate Temperatures

P. Chen, X. Wu, J. Lin,* K. L. Tan

Lithium- or potassium-doped carbon nanotubes can absorb ~20 or ~14 weight percent of hydrogen at moderate (200° to 400°C) or room temperatures, respectively, under ambient pressure. These values are greater than those of metal hydride and cryoadsorption systems. The hydrogen stored in the lithium- or potassium-doped carbon nanotubes can be released at higher temperatures, and the sorption-desorption cycle can be repeated with little decrease in the sorption capacity. The high hydrogen-uptake capacity of these systems may be derived from the special open-edged, layered structure of the carbon nanotubes made from methane, as well as the catalytic effect of alkali metals.

Hydrogen has been recognized as an ideal energy carrier, but to make it truly useful, end-user H_2 storage must be improved. In particular, high storage capacity is desirable when H_2 is used as the energy carrier in high-energy density rechargeable batteries and in H_2/O_2 fuel cells. For these applications, metal hydridation is the existing method above room temperatures and below 20 to 40 atm of pressure, but these materials are heavy and expensive (*1*, *2*). Cryoadsorption, in which activated carbon is often used as a sorbent, shows its advantages in the moderate size and weight of carbon, but suffers from the severe conditions (liquid nitrogen temperatures and 20 atm of pressure) required to hold the physically adsorbed H_2 (*3*, *4*). In any case, the H_2 uptake by these systems is less than 6 weight % (Table 1), far lower than that of gasoline or diesel (17.3 weight %). More recently, carbon nanotubes were reported to be a more effective material for H_2 uptake. Dollin *et al.* found that single wall carbon nanotube (SWNT) soots could absorb about 5 to 10 weight % of H_2 at 133 K and 300 torr (*5*). Chambers *et al.* observed that at 120 atm and room temperature, graphite nanofibers with herringbone structure could store 67 weight % of H_2 (*6*). Ye *et al.* used high-purity SWNT and obtained 8.25 weight % of H_2 adsorption at 80 K and 100 atm (*7*). All the above H_2-uptake systems require high pressure or subambient temperatures, or both. Here we introduce a H_2 storage system that uses alkali metal–doped carbon nanotubes (CNTs) as sorbents and operates at ambient pressure and moderate temperatures. The H_2 uptake can achieve 20 weight % for Li-doped CNT at 653 K, or 14 weight % for K-doped CNT at room temperature. These values correspond to ~160 (for Li-doped CNT) or 112 kg of H_2/m^3 (for K-doped CNT), respectively, and are comparable to those of gasoline and diesel.

Physics Department, National University of Singapore, 10 Kent Ridge Crescent, Singapore 119260.

*To whom correspondence should be addressed.

The CNTs used in this study were made from catalytic decomposition of CH_4 (*8*). After purification, almost all of the catalyst particles were removed. More than 90% of the product was in the form of multiwalled CNTs, and 70% was in the diameter range of 25 to 35 nm. The structure of a CNT is formed by the piling up of graphene sheets in the shape of circular cones with a hollow center. The doping of Li and K to the CNT was carried out by solid-state reactions between CNT and Li- or K-containing compounds, such as carbonates or nitrates. For comparison, Li- and K-doped graphite were prepared by the same procedures. The graphite sample was obtained from Merck with an average diameter of 50 μm. The specific surface area of CNT and graphite is 130 and 8.6 m^2/g, respectively. The Li/C and K/C ratio of these alkali-doped carbon materials was about 1/15 as measured by x-ray photoelectron spectroscopy. The density of Li-doped carbon materials was ~0.9 g/cm^3 for CNT and ~2.0 g/cm^3 for graphite. Hydrogen

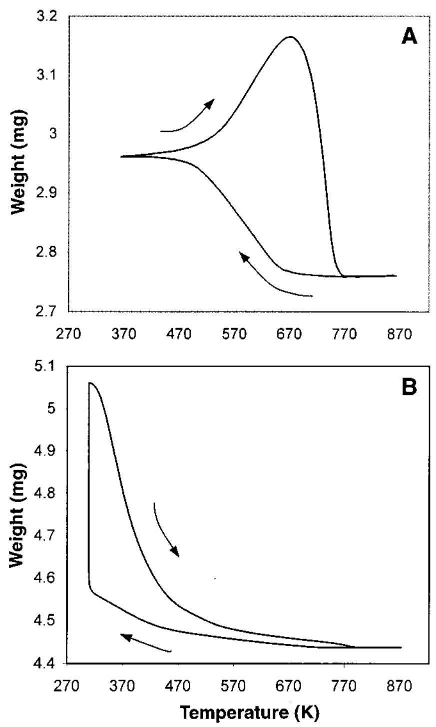

Fig. 1. TGA profile of a reversible H_2 sorption-desorption cycle on (**A**) Li-doped CNT and (**B**) K-doped CNT. Samples were initially treated at 873 K for 1 hour. For Li-doped CNT, the sample was cooled to 300 K, and then heated again to 873 K. For K-doped CNT, the sample was cooled to room temperature (298 K), maintained at 298 K for 2 hours, and then heated to 773 K.

uptake was measured by thermogravimetery analysis (TGA), with purified H_2 (>99.99%) as the purging gas. Hydrogen absorption-desorption was confirmed by temperature-programmed desorption (TPD), with H_2 being the only desorption product of the H_2-saturated carbons. In situ Fourier transform infrared spectroscopy (FTIR) was applied to analyze the detailed mechanism of the process. All the above investigations were performed mainly on Li-doped samples because they are stable under ambient conditions.

Samples for TGA were initially heated in situ at 873 K for 1 hour in a flow of purified H_2 (99.99%) to remove absorbed water and contaminants. The Li-doped samples were cooled from 873 to 300 K and then heated again to 873 K linearly (5° per minute). The H_2 uptake began at temperatures around 773 K and ended at 423 K (Fig. 1A). When the temperature was increased again, the sample further increased its weight, reaching a maximum value corresponding to a total of 14.5 weight % H_2 at 673 K. Further increasing the temperature resulted in the H_2 desorption, and the sample weight returned to its original value at 773 K. In the above hydrogenation-dehydrogenation cycle, the system did not reach the equilibrium (saturation) state.

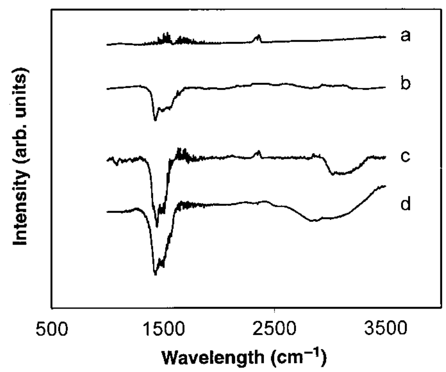

Fig. 2. FTIR spectra of (a) CNT at 650 K, and (b to d) Li-doped CNT in the H_2 stream at 873 K for 1 hour, 650 K for 1 hour, and 650 K more than 2 hours, respectively.

When the Li-doped CNT sample was maintained at 653 K for 2 hours, the H_2 uptake reached 20 weight % H_2 at ambient pressure.

The K-doped samples were cooled from 873 K to room temperature in a H_2 stream and maintained at room temperature for 2 hours. They were then heated again at 5° per minute to 773 K. A gradual weight increase was observed from 773 to 343 K (Fig. 1B). As the temperature was further decreased, a rapid weight increase occurred that reached ~14 weight % (saturated value) after the system was maintained at room temperature for 2 hours. Desorption of H_2 took place as the temperature was raised. The desorption was rapid between 300 and 423 K and then became relatively gradual. It appears that there are at least two kinds of absorbed H_2 in K-doped CNT that desorb in temperature regimes.

Similar H_2 uptake was observed for Li- and K-doped graphite, but the H_2 uptake by alkali-doped graphite was only 35 to 70% of that by alkali-doped CNT (Table 1). It seems that H_2-uptake capacity correlates with the structure of carbon sorbents. Compared with graphite, the carbon nanotubes used in this work consist of small-sized graphene sheets (50 nm or less) in the shape of a hollow circular cone and have much more open edge and greater interplanar distance (0.347 nm for CNT versus 0.335 nm for graphite). All these features favor the high H_2 uptake by alkali-doped CNT.

Compared with 0.4 weight % or no H_2 absorption measured for the same carbon nanotubes or graphite sample without alkali doping (*9*), the high H_2-uptake capacity may derive from the properties of alkali metals. Our in situ FTIR investigation has unambiguously shown that the H_2 uptake under the conditions used in this study (ambient pressure, moderate temperatures, presence of alkali metals) is actually a dissociative hydrogenation of the carbon sorbents. When H_2 uptake was not evident at temperatures above 773 K, there was only weak Li-H vibration at ~1420 cm^{-1} (Fig. 2, curve b). As the temperature was reduced to 653 K, the Li-H vibration became more intense and a weak band, which is due to C-H stretching, developed between 3000 and 3350 cm^{-1} (curve c). When the sample was kept in contact with H_2 at 653 K for hours, the C-H band appeared gradually and broadened, whereas no significant change in the Li-H vibration was observed (Fig. 2, curve d). The infrared absorption corresponding to C-H stretching in alkanes occurs in the range of 2840 to 3000 cm^{-1}, whereas in cyclic alkanes or alkenes absorption it is between 3000 and 3300 cm^{-1} (*10*). This newly developed band at 2600 to 3400 cm^{-1} therefore revealed the formation of CH_x species, indicating that the adsorption resulted from the dissociative hydrogenation of carbon nanotubes or graphite. Upon heating to high temperatures at which the H_2 desorption took place, the C-H band correspondingly vanished.

The formation of the LiH species was observed by FTIR to occur before C-H formation, and it maintained constant intensity, whereas the C-H band increased with increasing H_2 exposure. This suggests that Li may act as a catalytic active center for the H_2-dissociative adsorption. The dissociated H atoms may spill over from Li sites to the carbon network of grapheen sheets, and finally become bonded to carbon atoms. Our x-ray

Table 1. Comparison of H_2 storage properties of various systems. W_i: H_2-uptake capacity (weight % H_2); V_i: H_2 density (g/liter).

System	T_{absorb} (K)	P_{absorb} (atm)	H_2 density		Energy density	
			W_i	V_i	kWh/Kg	kWh/liter
CNT	298–773	1	0.4	3.2	0.133	0.106
Li-doped						
CNT	473~673	1	20.0	180	6.66	6.0
Graphite	473~673	1	14.0	280	4.66	9.32
K-doped						
CNT	<313	1	14.0	12.6	4.66	4.2
Graphite	<313	1	5.0	60	1.66	2.0
FeTi-H	>263	25	<2	96	0.58	3.18
NiMg-H	>523	25	<4	81	1.05	2.69
Cryoadsorption	~77	20	~5	~20	1.66	0.67
Isooctane/gasoline	>233	1	17.3	117	12.7	8.76

diffraction measurement revealed the formation of Li_2C_2 in the Li-doped CNT or graphite. We have also performed ultraviolet photoelectron spectroscopy (UPS) studies of valence band structure for both samples with and without Li. It was shown that the Li doping resulted in an extra half-filled electron-density-of-state containing the Fermi edge (*11*). The H_2-dissociative adsorption on carbon is a slow activated process (*12*), with an activation energy corresponding to an above-zero-energy crossing between the di-H atoms and H_2 molecular potential curves. Theoretical band-structure calculation (*13*) has indicated that the half-filled Fermi level band created by the Li doping can overlap strongly with the unoccupied antibonding H_2 $(1s^2)^*$ orbital, which to a large extent reduces the energy barrier for H_2 dissociation. We can therefore observe the high H_2 uptake resulting from Li doping.

The H_2-rechargeability of Li- and K-doped samples was tested by TGA. For Li-doped samples (CNT and graphite), the saturated H_2 uptake was measured at 653 K after each complete desorption at 823 K, whereas for K-doped carbon materials it was measured at 298 K after each run of desorption at 773 K. The results show that after more than 20 cycles of absorption-desorption, the capacities of H_2 uptake are reduced by less than 10% for both systems. High H_2 pressure was shown to favor the H_2 absorption, which is expected because H_2 uptake is a volume-reducing process. TPD measurements have demonstrated that the Li-doped CNT exposed to H_2 at 10 atm for 1 hour can store the same amount of H_2 as those systems at ambient pressure for 2 hours.

Although K-doped carbon samples can absorb H_2 at lower temperature than Li-doped samples, Li-doped carbon materials are chemically more stable than K-doped carbon materials. They can maintain H_2 uptake capability even after being heated in air at 373 K for hours, and no flame resulted even when the samples were exposed to air at 673 K after H_2 had been absorbed. On the other hand, K-doped CNT can be oxidized rapidly and even cause fire shortly after being exposed to air at room temperature. Nevertheless, both systems may find wide applications in the near future.

References and Notes

1. G. C. Carter and F. L Carter, *Metal-Hydrogen Systems*, T. Nejat Veziroglu, Ed. (Pergamon, Oxford, 1981), chap. 7.
2. H. Buchner, P. Pelloux-Gervais, M. Müller, F. Grafwallner, P. Luger, *Hygrogen and Other Alternative Fuels for Air and Ground Transportation*, H. W. Pohl, Ed. (Wiley, Chichester, UK, 1995), chaps. 7 to 11.
3. J. Nitsch, W. Peschka, W. Schnurnberger, M. Fischer, H. Eichert, in *Hydrogen as an Energy Carrier*, C. Winter and J. Nitsch, Eds. (Springer-Verlag, Berlin, 1988), part B.
4. S. Hynek, W. Füller, J. Bentley. *Int. J. Hydrogen Energy* **22**, 601 (1997).
5. A. C. Dillon, K. M. Jones, T. A. Bekkedahl, C. H. Kiang, D. S. Bethuune, M. J. Heben, *Nature*, **386**, 377 (1997).
6. A. Chambers, C. Park, R. T. K. Baker, *J. Phys. Chem. B* **102**, 4253 (1998).
7. Y. Ye *et al.*, *Appl. Phys. Lett.*, **74**, 2307 (1999).
8. P. Chen, X. Wu, J. Lin, K. L. Tan, *Phys. Rev. Lett.* **82**, 254 (1999); P. Chen, H. B. Zhang, G. D. Lin, Q. Hong, K. R. Tsai, *Carbon* **35**, 1495 (1997).
9. X. Wu, P. Chen, J. Lin, K. L. Tan, *Int. J. Hydrogen Energy*, in press.
10. R. M. Silverstein, G. C. Bassler, T. C. Morrill, *Spectrometric Identification of Organic Compounds* (Wiley, New York, 1991), pp. 103–107.
11. R. Schlagl, in *Progress in Intercalation* Research, W. Müller-Warmuth and R. Schollorn, Eds. (Kluwer, Dordrecht, Netherlands, 1994), pp. 83–176.
12. R. I. Masel, *Principles of Adsorption and Reaction on Solid Surfaces* (Wiley, New York, 1996), p. 443.
13. N. A. Holzwarth, S. Rabii, L. A. Girifalco, *Phys. Rev. B* **18**, 5190 (1978).

12 January 1999; accepted 1 June 1999

Regulation of NMDA Receptors by an Associated Phosphatase-Kinase Signaling Complex

Ryan S. Westphal,[1]* Steven J. Tavalin,[1]* Jerry W. Lin,[2] Neal M. Alto,[1] Iain D. C. Fraser,[1] Lorene K. Langeberg,[1] Morgan Sheng,[2] John D. Scott[1]†

Regulation of *N*-methyl-D-aspartate (NMDA) receptor activity by kinases and phosphatases contributes to the modulation of synaptic transmission. Targeting of these enzymes near the substrate is proposed to enhance phosphorylation-dependent modulation. Yotiao, an NMDA receptor–associated protein, bound the type I protein phosphatase (PP1) and the adenosine 3′,5′-monophosphate (cAMP)–dependent protein kinase (PKA) holoenzyme. Anchored PP1 was active, limiting channel activity, whereas PKA activation overcame constitutive PP1 activity and conferred rapid enhancement of NMDA receptor currents. Hence, yotiao is a scaffold protein that physically attaches PP1 and PKA to NMDA receptors to regulate channel activity.

The molecular organization of the postsynaptic density (PSD) is thought to be essential for the fidelity and precision of synaptic signaling events. Clustering and immobilization of neurotransmitter receptors and ion channels is maintained by an intricate system of protein-protein interactions (*1*). For example, NMDA receptors are clustered and coupled to the cytoskeleton through association with PDZ domain–containing proteins, α-actinin, and neurofilaments (*2*). Many signaling pathways converge on the NMDA receptor (*3*), allowing the regulation of channel activity in response to the generation of second messengers such as Ca^{2+} and cAMP (*4, 5*). PKA and PP1 activities modulate NMDA receptor function and appear to act in opposition to each other (*5, 6*). Individual targeting or anchoring proteins such as AKAP79 and spinophillin localize the kinase and phosphatase at the PSD (*7, 8*).

A two-hybrid screen for proteins that bind the NMDA receptor subunit isoform NR1A identified a protein called yotiao that interacts with the COOH-terminal C1 exon cassette of the ion channel (*9*). We isolated cDNAs encoding fragments of yotiao by an interaction cloning strategy to identify A-kinase anchoring proteins (AKAPs) (*10*) and confirmed that the protein bound NR1A (*11*). Expression of full-length yotiao fused to green fluorescent protein (GFP) in HEK 293 cells (*12*) resulted in detection of a ~210-kD protein that bound the type II regulatory subunit of PKA (RII), as assessed by overlay assay (Fig. 1A). Immunoprecipitations with antiserum to yotiao from brain extracts also isolated an RII binding protein and were enriched by a factor of 10.5 ± 2 ($n = 3$) for PKA catalytic subunit activity (Fig. 1, B and C). We mapped the RII binding site to a region between residues 1229 and 1480 by screening a family of recombinant yotiao fragments (Fig. 1D) in the overlay assay (Fig. 1, E and F). Residues 1440 to 1457 appear to include the principal determinants for RII interaction because a synthetic peptide encompassing this region blocked RII binding (Fig. 1F). These findings indicate that yotiao functions to anchor PKA to NMDA receptors.

Because PP1 activity participates in the regulation of NMDA receptors (*6*), we conducted experiments to address whether the

[1]Howard Hughes Medical Institute, Vollum Institute, Oregon Health Sciences University, 3181 S.W. Sam Jackson Road, Portland, OR 97201, USA. [2]Howard Hughes Medical Institute and Department of Neurobiology, Massachusetts General Hospital and Harvard Medical School, Boston, MA 02114, USA.

*These authors contributed equally to this article.
†To whom correspondence should be addressed. E-mail: scott@ohsu.edu